Supporting Information

Microstructure and Lattice Strain Control towards High-Performance Ambient Green-Printed Perovskite Solar Cells

Junjie Fang,[a] Zicheng Ding,*[a] Xiaoming Chang,[a] Jing Lu,[a] Tinghuan Yang,[a] Jialun Wen,[a] Yuanyuan Fan,[a] Yalan Zhang,[a] Tao Luo,[a] Yonghua Chen,*[b] Shengzhong (Frank) Liu*[ac] and Kui Zhao*[a]

[a]Key Laboratory of Applied Surface and Colloid Chemistry, Ministry of Education; Shaanxi Key Laboratory for Advanced Energy Devices; Shaanxi Engineering Lab for Advanced Energy Technology, School of Materials Science and Engineering, Shaanxi Normal University, Xi'an 710119, China

*E-mail: zcding@snnu.edu.cn; szliu@dicp.ac.cn; zhaok@snnu.edu.cn

[b]Key Laboratory of Flexible Electronics (KLOFE) & Institution of Advanced Materials (IAM), Nanjing Tech University (NanjingTech), Nanjing 211816, China

*E-mail: iamyhchen@njtech.edu.cn

[c]Dalian National Laboratory for Clean Energy; iChEM, Dalian Institute of Chemical Physics, Chinese Academy of Sciences, Dalian 116023, China

Experimental Method

Materials: The SnO_2 precursor (Tin(IV) oxide, 15% in H_2O colloidal dispersion), guanidinium iodide (GAI, 99.5%.) and lead iodide (PbI_2, 99.9985%) were purchased from Alfa Aesar. Methylammonium iodide (MAI, 99.5%), methylammonium bromide (MABr, 99.5%), methylammonium acetate (MAAc, 99.5%) and ethyl acetate (EA, 99.5%) were purchased from Xi'an Polymer Light Technology Corp. 2,2',7,7'-tetrakis-(N,N-di-p-methoxyphenylamine)-9,9'-spirobifluorene (spiro-OMeTAD) (≥99.0%) was purchased from Shenzhen Feiming Science and Technology Co., Ltd. All the chemicals were used as received without further purification.

Solution preparation: The perovskite precursor solution was prepared by dissolving GAI (0.072 mol), MAI (0.528 mol) and PbI_2 (0.6 mol) in 1 mL MAAc. The blend was stirred at 60 ºC for 12 h to ensure the complete dissolution. MABr additive with molar ratios of 0%, 4%, 8% and 12% (MABr:Pb) was incorporated into the perovskite precursor solution. The spiro-OMeTAD solution was consisted of 40 mg spiro-OMeTAD, 22 μL lithium bis(trifluoromethanesulfonyl) imide solution (520 mg in 1 ml acetonitrile) and 36 μL 4-tert-butylpyridine and 1 mL EA solvent. The purchased SnO_2 precursor solution was diluted by water in 8-fold prior to use.

Device fabrication and characterization: The fluorine doped tin oxide (FTO) glass substrates (2.9 cm × 2.9 cm) was cleaned by sonicating in acetone, isopropanol and ethanol sequentially. The substrates were then dried in a N_2 flow, ant treated by O_3 plasma for 18 min before use. The ETL, perovskite layer and HTL are prepared by blade coating at a speed of 1 m min^{-1} in ambient conditions. The SnO_2 ETL was

fabricated by blade coating the diluted solution on the pre-heated substrate at 100 ºC, and then annealing the coated film at 150°C for 30 min. The perovskite layer of $GA_{0.12}MA_{0.88}PbI_3$ was obtained by blade coating the precursor solution with different substrate temperature (130, 160, 190 and 210 ºC), and then annealed at 100°C for 10 min. The perovskite films with different content of MABr additive (0%, 4%, 8% and 12%) were obtained similarly and the substrate temperature was fixed at 190 ºC. The spiro-OMeTAD HTL was blade-coated at 40 ºC and then stored in an auto-drying cabinet at 20 °C with a relative humidity of 15% for 8 h. Finally, a 100-nm thick gold electrode was evaporated on the top of HTL to complete the device. The *J–V* characteristics of the solar cells were analysed using a Keithley 2400 SourceMeter under simulated 1-sun AM1.5G illumination at 100 mW cm^{-2} (Oriel solar simulator) in ambient conditions at room temperature. A metal aperture of 0.09 cm^2 was used to define the active area. The scan ranges from 2.5 V to –0.1 V with a bias step of 0.02 V. The light intensity was calibrated using an NREL-traceable KG5-filtered silicon reference cell. The external quantum efficiency (EQE) was characterized on a QTest Station 2000ADI system (Crowntech Inc., USA) with a 300-W xenon lamp as the light source. The monochromatic light intensity was calibrated with a reference silicon photodiode.

Film characterization: X-ray diffraction (XRD) was performed on a Rigaku Smart Lab (X-ray Source: Cu Kα, λ = 1.54 Å). In Williamson-Hall analysis, the strain (ε) is derived from the following equation: $\beta cos\theta = \frac{k\lambda}{D} + 4\varepsilon sin\theta$, where β is the crystallite size and can be calculated from the full width at half maximum (FWHM) of the peaks (110) (112)

(211) (202) (220) (310), θ is Bragg diffraction angle, k is Scherrer constant, λ is X-ray wavelength, and D is the average thickness of the crystal grain perpendicular to the crystal plane. Fourier transform infrared (FTIR) spectra were measured with a Bruker Vertex 70. The scanning electron microscopy (SEM) was characterized using a FE-SEM (SU-8020, Hitachi). Femtosecond pump-probe transient absorption (front-side excitation) measurements were performed by using a commercial TA system (Time-Tech Spectra, LLC). The femtosecond laser pulse was generated by solid-state diode pump regeneration amplifier with 1030 nm wavelength and 100 kHz repetition rate (light conversion) and served as both pump and probe beams. Femtosecond pump-probe transient absorption measurements were performed at appropriate power density (16.64 μJ cm^{-2}) at room temperature. The pump pulse with a wavelength of 500 nm and duration of 290 fs generated via a second harmonic generator (SHG) was used to excite all the samples and the probe beam (from 600 to 900 nm) was detected by a high-speed spectrometer. The samples for XRD, SEM, absorption and FTIR characterization were blade-coated on FTO/SnO_2 layer. The electrical impedance spectroscopy (EIS) of the completed devices were measured on an electrochemical workstation (IM6ex, Zahner, Germany) under open-circuit conditions in dark. The frequency ranges from 10 Hz to 4 MHz. The steady-state photoluminescence (PL) and time-resolved photoluminescence (TRPL) (excitation at 510 nm, front-side excitation) were measured on PicoQuant FT-300 spectrometer with an excitation wavelength at 510 nm from front-side, and the samples were blade-coated at glass side. The carrier lifetime was determined using the following equation:

$$F(t) = \sum A_i \, exp(-\frac{t}{\tau_i}) + A_0$$

where A_i and τ_i are the amplitude and carrier lifetime of the i_{th} process, and A_0 is the background signal intensity. The average carrier lifetime was calculated according to the following equation:

$$\tau_{ave} = \frac{\sum A_i \tau_i^2}{\sum A_i \tau_i}$$

Charge mobility measurement: The electron-only devices were fabricated based on the configuration of FTO/SnO_2/Perovskite/PCBM/Ag. The dark *I–V* characteristics were measured on a Keithley 2400 SourceMeter. The trap density was determined using the following equation:

$$n_{trap} = \frac{2\varepsilon_0 \varepsilon_r V_{TFL}}{eL^2}$$

where ε_0 is the vacuum permittivity, ε_r is the relative dielectric constant, V_{TFL} is the onset voltage of the trap-filled limit region, *e* is the elementary charge, and *L* is the distance between the electrodes. The electron mobility was further extracted using the Mott-Gurney law:

$$\mu = \frac{8 J_D L^3}{9 \varepsilon_0 \varepsilon_r V^2}$$

where J_D is the current density and *V* is the applied voltage.

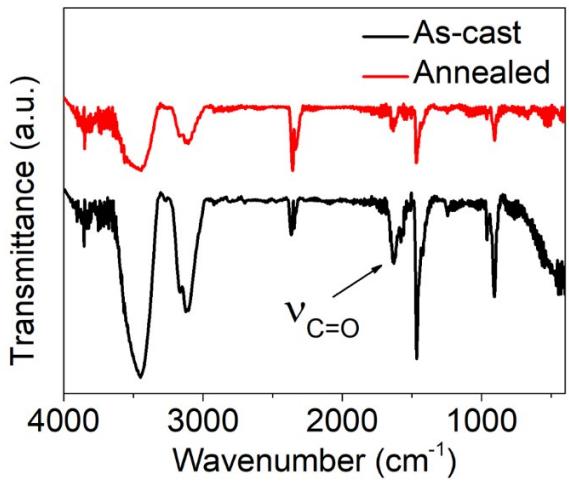

Fig. S1 FTIR spectra of the as-cast and annealed blade-coated $GA_{0.12}MA_{0.88}PbI_3$ film with MAAc as processing solvent. The substrate temperature is 190 °C, and the annealing temperature is 100 °C.

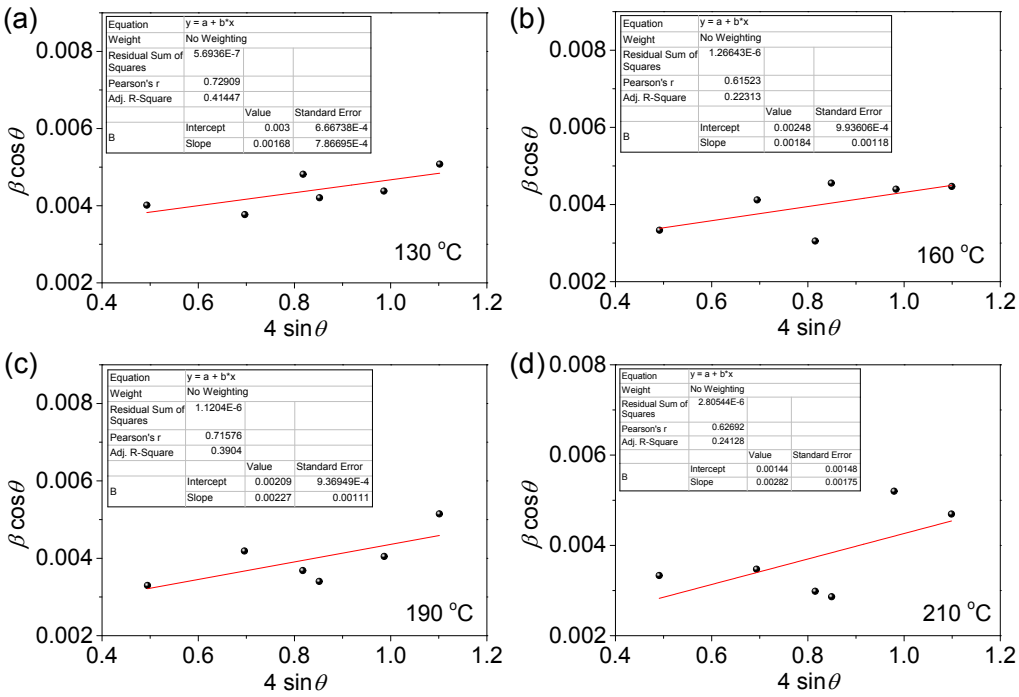

Fig. S2 Williamson−Hall analysis of the $GA_{0.12}MA_{0.88}PbI_3$ films at different temperatures.

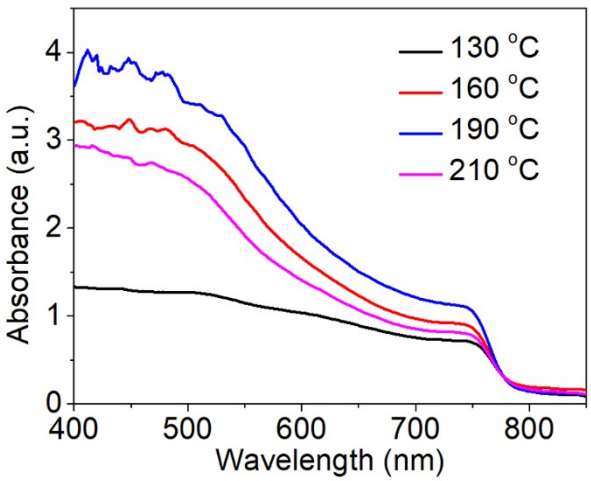

Fig. S3 Absorption spectra of the $GA_{0.12}MA_{0.88}PbI_3$ films at different temperatures on glass substrates.

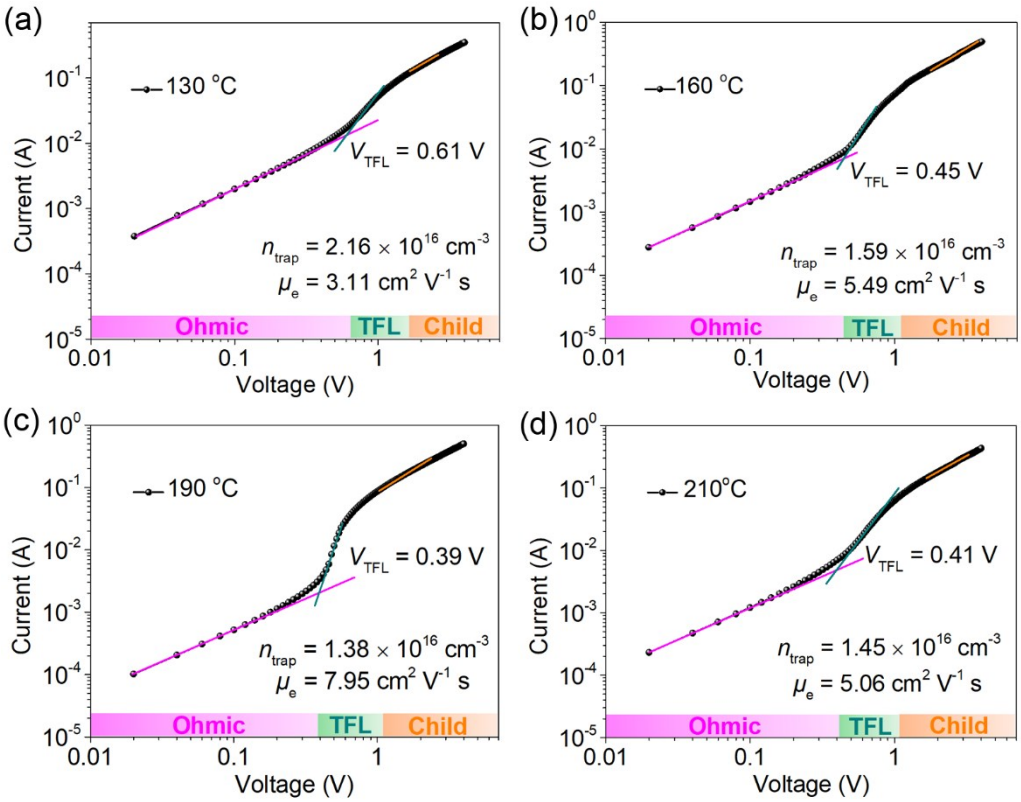

Fig. S4 Dark *I–V* measurement of the electron-only device based on the $GA_{0.12}MA_{0.88}PbI_3$ films at different temperatures.

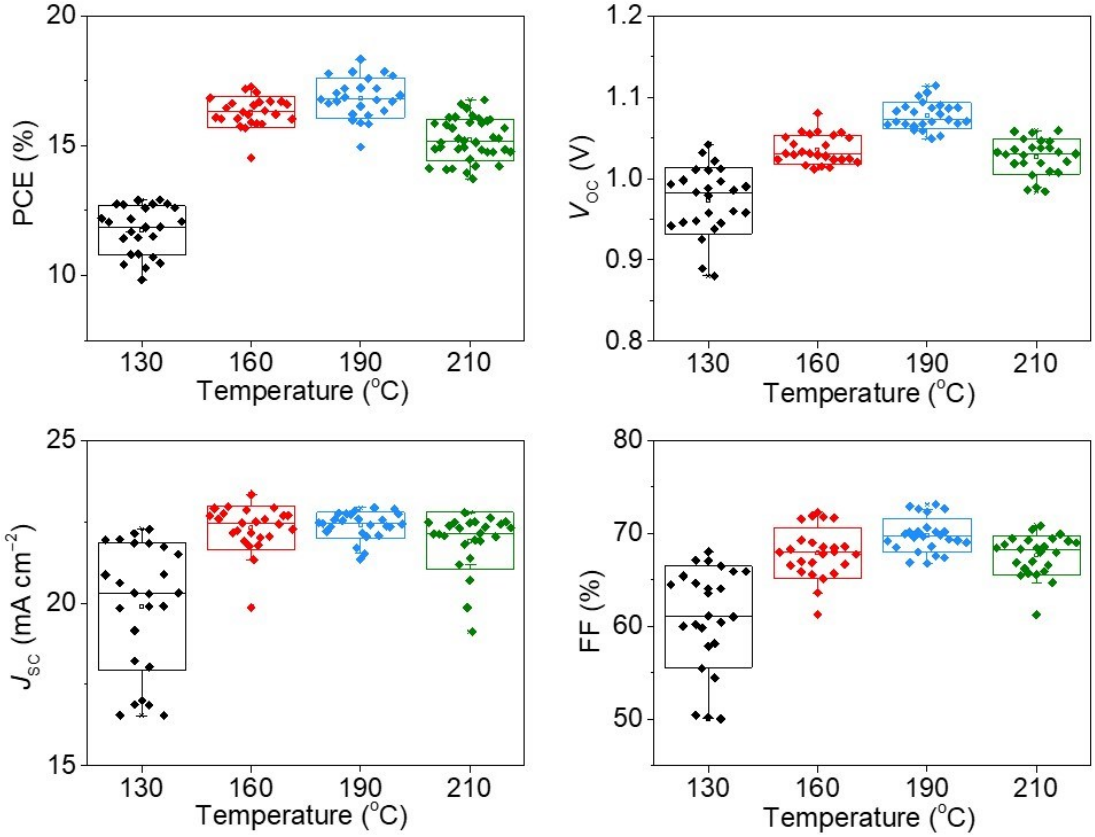

Fig. S5 Distributions of PCE, V_{OC}, J_{SC} and FF for the PSC devices based on the $GA_{0.12}MA_{0.88}PbI_3$ films at different temperatures from 25 individual devices.

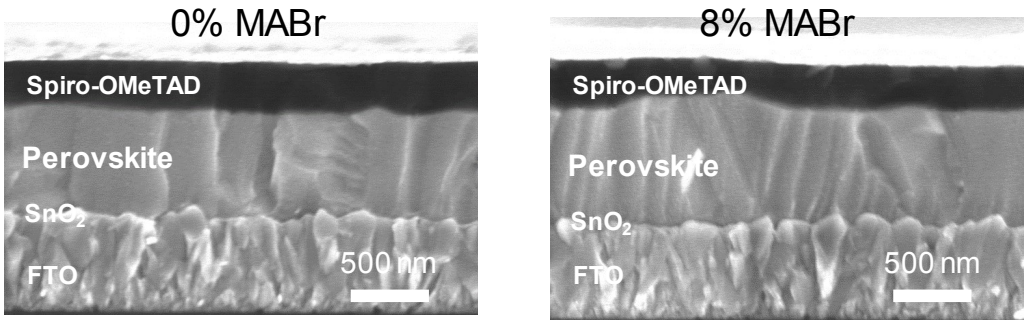

Fig. S6 Cross-sectional SEM images of the PSC devices from the blade-coated $GA_{0.12}MA_{0.88}PbI_3$ film without and with 8% MABr.

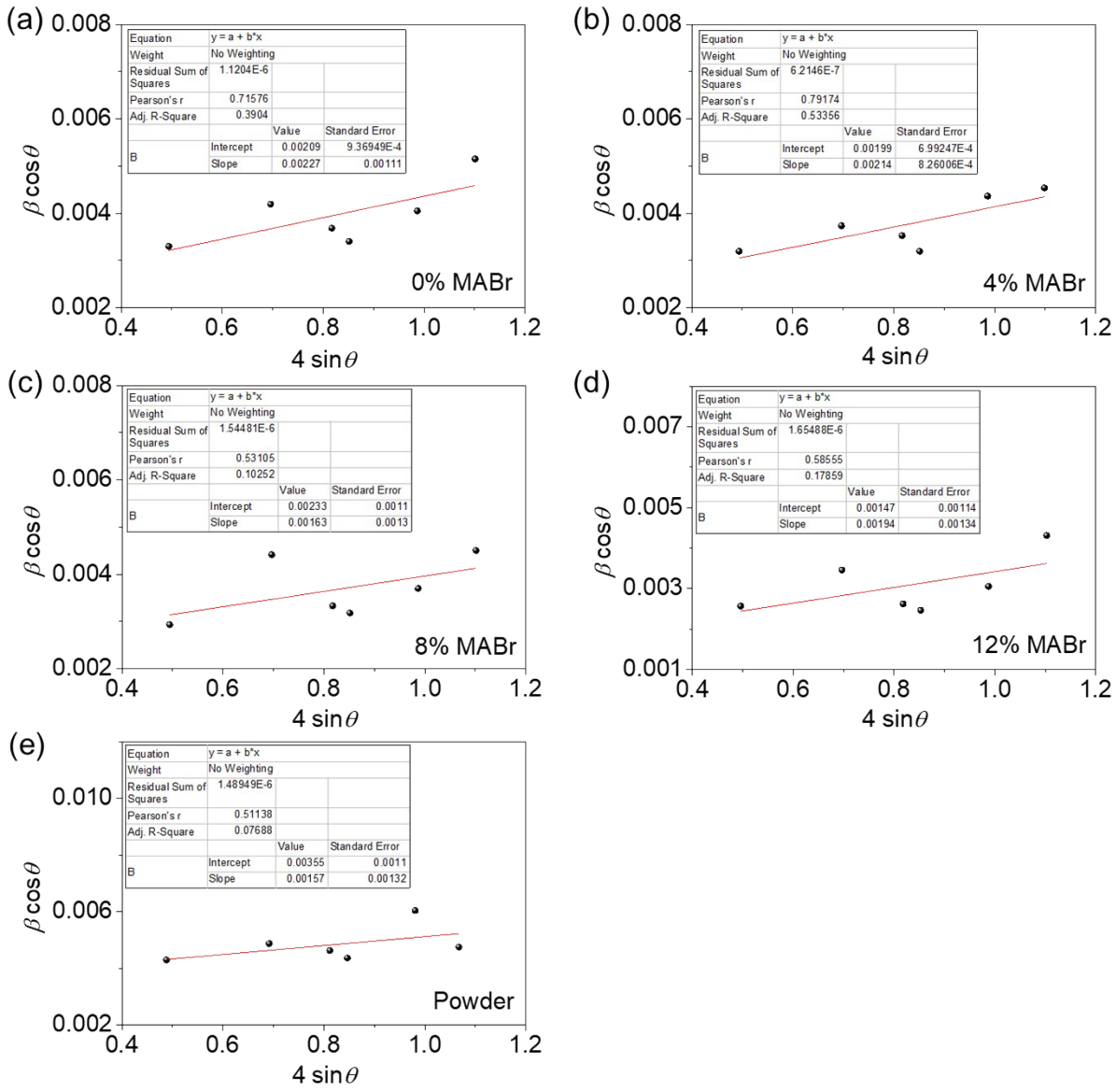

Fig. S7 Williamson−Hall analysis of the $GA_{0.12}MA_{0.88}PbI_3$ films with different content of MABr (a-d) and the scraped perovskite powder without MABr (e).

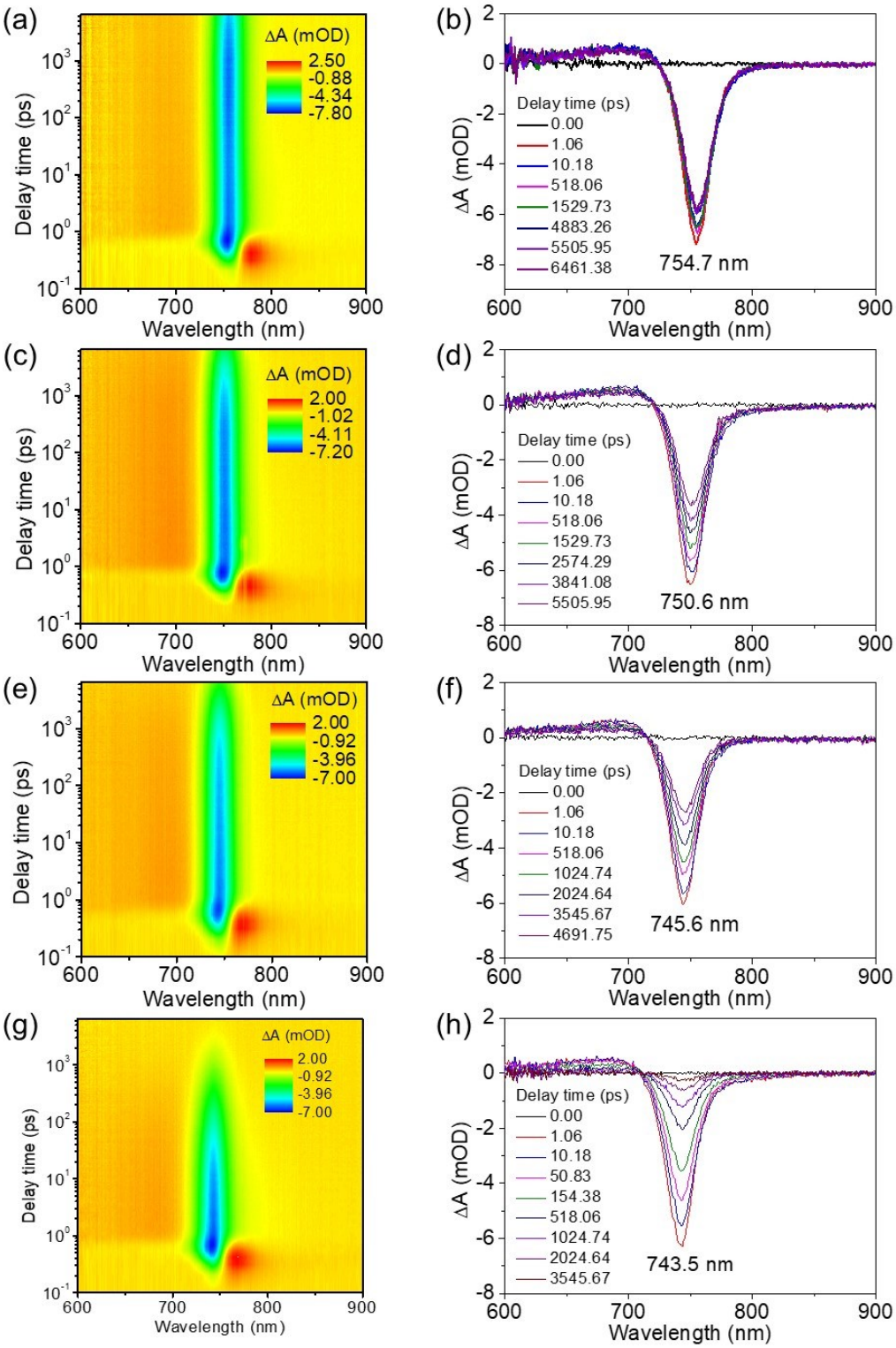

Fig. S8 2D pseudocolor TA spectra of the perovskite films with different content of MABr after excitation at 500 nm as a function of probe wavelength and probe delay time: (a) 0% MABr, (c) 4% MABr, (e) 8% MABr, (g) 12% MABr. (b), (d), (f) and (h) are the corresponding ΔA spectra of (a), (c), (e) and (g) at different delay time.

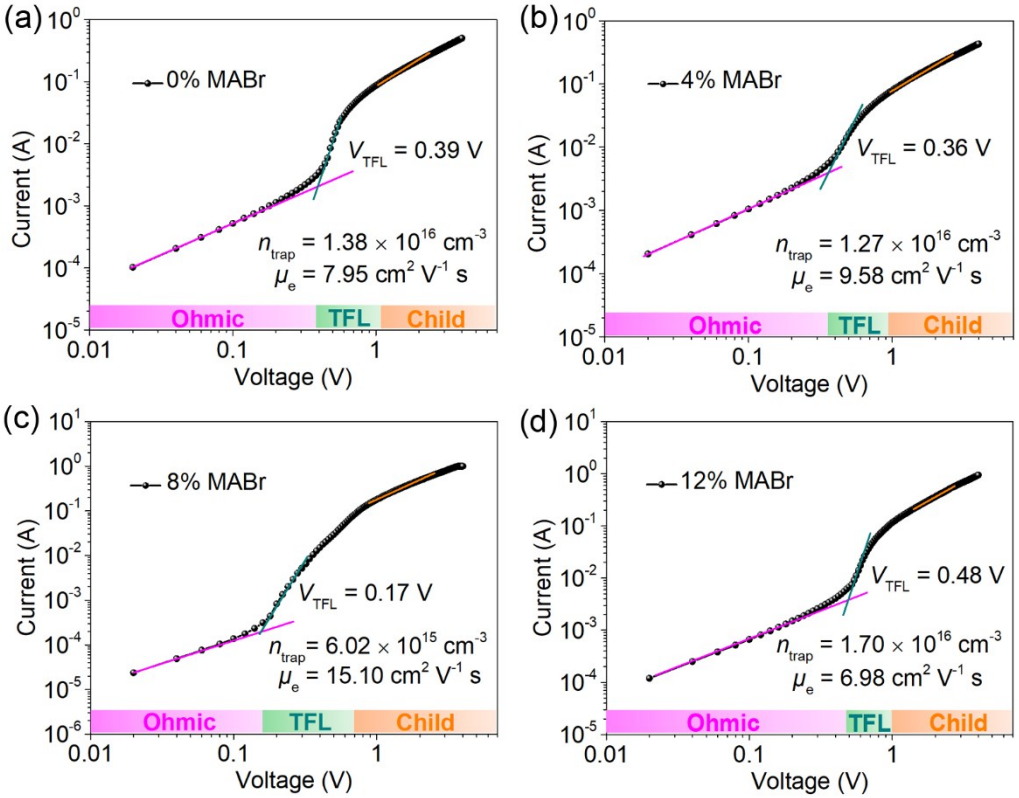

Fig. S9 Dark *I–V* measurement of the electron-only device based on the $GA_{0.12}MA_{0.88}PbI_3$ films with different content of MABr.

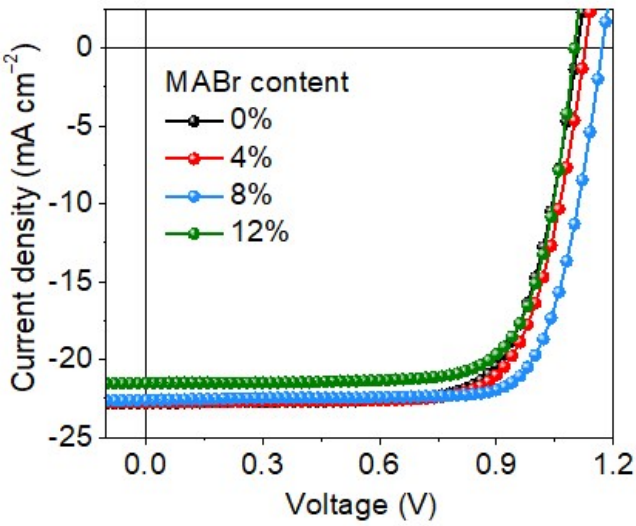

Fig. S10 The *J–V* curves of the PSCs based on the films with different content of MABr.

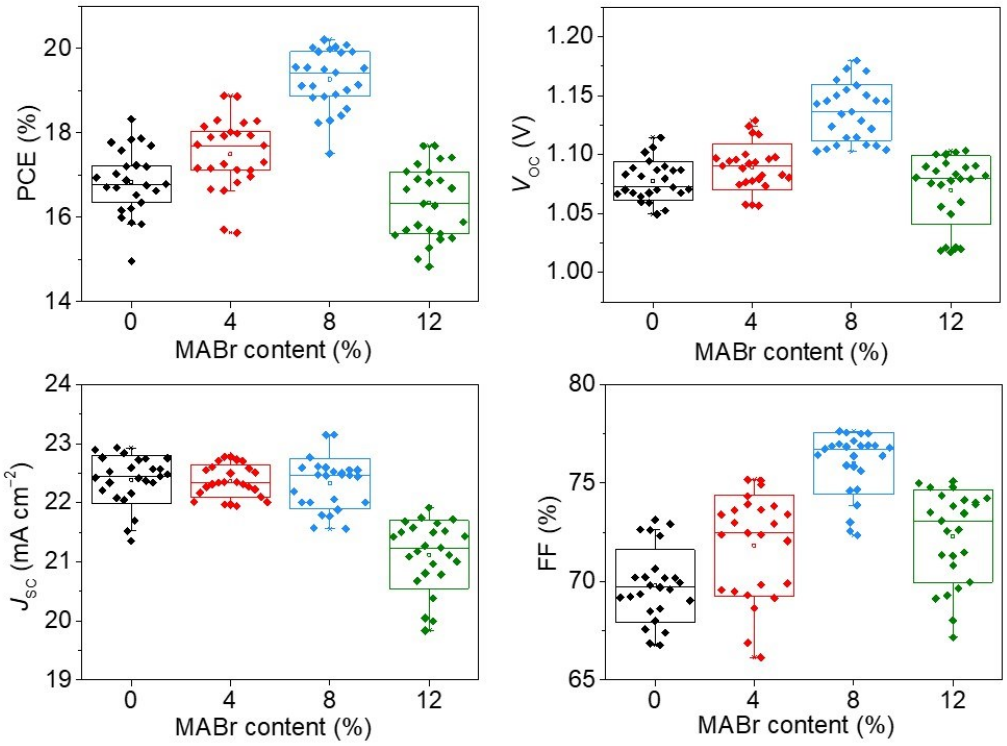

Fig. S11 Distributions of PCE, V_{OC}, J_{SC} and FF for the PSC devices based on the films with different content of MABr from 25 individual devices.

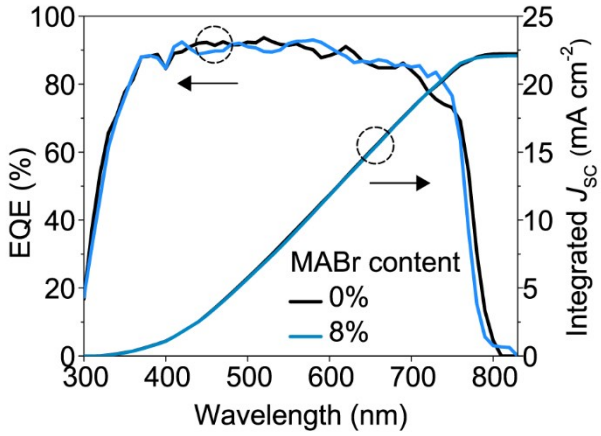

Fig. S12 EQE spectra and integrated J_{SC} of the champion devices without and with 8% MABr.

Supporting Table S1. The fitting parameters of TRPL spectra for the $GA_{0.12}MA_{0.88}PbI_3$ films processed at different temperatures.

Temperature (°C)	A_1	τ_1 (ns)	A_2	τ_2 (ns)	τ_{ave} (ns)
130	0.9627	146.60	0.0373	3.10	141.24
160	0.9079	228.50	0.0921	48.03	211.88
190	0.9213	303.67	0.0787	40.32	282.94
210	0.9795	157.59	0.0205	3.75	154.43

Supporting Table S2. The fitting parameters of TRPL spectra for the $GA_{0.12}MA_{0.88}PbI_3$ films with different MABr content.

MABr content	A_1	τ_1 (ns)	A_2	τ_2 (ns)	τ_{ave} (ns)
0%	0.9213	303.67	0.0787	40.32	282.94
4%	0.9745	431.18	0.0255	43.36	421.30
8%	0.9727	464.90	0.0273	59.98	453.84
12%	0.9680	383.39	0.0320	43.86	372.54

Supporting Table S3. The EIS parameters for the completed PSC devices based on the perovskite films with different content of MABr.

MABr content	R_s (Ω)	C_{rec} (nF)	R_{rec} (Ω)
0%	9.1	168.9	28.0
4%	8.7	311.7	35.8
8%	5.7	102.5	40.6
12%	6.7	236.2	34.0

Supporting Table S4. The photovoltaic parameters comparison of this work with other state-of-art solution-processed $MAPbI_3$-based PSCs.

Method	Toxicity	Solvent	V_{OC} (V)	J_{SC} (mA cm^{-2})	FF (%)	PCE (%)	Reference
Spin-coating	Toxic	DMF, DMSO, CB	1.10	21.81	79.39	19.18	[1]
		GBL, ACN	1.12	23.46	78.9	20.63	[2]
		DMF, DMSO, Toluene	1.116	23.5	82	21.6	[3]
		DMF, NMP	1.10	21.01	80.13	18.50	[4]
		DMF, DMSO, DEE	1.10	22.69	84.07	21.01	[5]
		DMF, aniline	1.112	22.983	80.8	20.65	[6]
		DMF, DMSO, toluene	1.15	22.7	80.9	21.1	[7]
		DMSO, DMF, IPA	1.12	23.83	79.09	21.08	[8]
		DMF, DMSO, toluene	1.07	22.8	82.2	20.05	[9]
		DMF, GBL, toluene	1.111	23.11	76.75	19.71	[10]
		DMF, DMSO, CB	1.14	22.57	78	20.18	[11]
Spin-coating	Green	MAAc	1.11	23.16	78.01	20.05	[12]
		ACN (with CH_3NH_2 gas)	1.12	22.39	77.7	20.26	[13]
Printing	Toxic	DMF, DMSO	1.09	21.98	81	19.41	[14]
		DMF	1.18	22.5	81.7	21.7	[15]
		NMP, DMF	1.097	22.53	77.1	19.06	[16]
		DMF, DMSO, CB	1.10	22.7	81	20.2	[17]
		DMF, DMSO, IPA	1.03	21.36	76	16.71	[18]
		DMF, DMSO, CB	1.09	23.46	78.51	20.08	[19]
		IPA, DMF, GBL	1.10	21.4	77.6	18.3	[20]
		DMF, DMSO, IPA	1.08	22.66	76.2	18.64	[21]
		DMF, DMSO, DEE	1.07	20.7	77.1	17.2	[22]
		2-methoxyethanol	1.19	21.03	78	19.44	[23]
		2-methoxyethanol, ACN	1.13	23.0	81.8	21.3	[24]
Printing	Green	tetrahydrofuran, methylamine, ethanol	1.09	23.86	77	20.02	[25]
		ACN, methylamine, methanol	1.09	24.93	78.61	21.12	[26]
		MAAc	1.17	22.60	76.37	20.21	This work

Notes: DMF refers to N,N-dimethylformamide, DMSO refers to dimethylsulfoxide, CB refers to chlorobenzene, GBL refers to γ-butyrolactone, ACN refers to acetonitrile, NMP refers to N-methyl-2-pyrrolidone, DEE refers to diethyl ether, IPA refers to isopropanol.

Supporting References

1 B. Kim, M. Kim, J. H. Lee and S. I. Seok, *Adv. Sci.*, 2020, **7**, 1901840.

2 Y. Hou, K. Wang, D. Yang, Y. Jiang, N. Yennawar, K. Wang, M. Sanghadasa, C. Wu and S. Priya, *ACS Energy Lett.*, 2019, **4**, 2646–2655.

3 H. Chen, Q. Wei, M. I. Saidaminov, F. Wang, A. Johnston, Y. Hou, Z. Peng, K. Xu, W. Zhou, Z. Liu, L. Qiao, X. Wang, S. Xu, J. Li, R. Long, Y. Ke, E. H. Sargent and Z. Ning, *Adv. Mater.*, 2019, **31**, 1903559.

4 G. Jang, H. C. Kwon, S. Ma, S. C. Yun, H. Yang and J. Moon, *Adv. Energy Mater.*, 2019, **9**, 1901719.

5 Z. Li, F. Wang, C. Liu, F. Gao, L. Shen and W. Guo, *J. Mater. Chem. A*, 2019, **7**, 22359–22365.

6 Y. Wang, T. Li, Z. Li, S. Wang and X. Deng, *Adv. Funct. Mater.*, 2019, **29**, 1903330.

7 Y. Bai, Y. Lin, L. Ren, X. Shi, E. Strounina, Y. Deng, Q. Wang, Y. Fang, X. Zheng, Y. Lin, Z.-G. Chen, Y. Du, L. Wang and J. Huang, *ACS Energy Lett.*, 2019, **4**, 1231–1240.

8 S. Wang, H. Chen, J. Zhang, G. Xu, W. Chen, R. Xue, M. Zhang, Y. Li and Y. Li, *Adv. Mater.*, 2019, **31**, 1903691.

9 B. Wang, F. Wu, S. Bi, J. Zhou, J. Wang, X. Leng, D. Zhang, R. Meng, B. Xue, C. Zong, L. Zhu, Y. Zhang and H. Zhou, *J. Mater. Chem. A*, 2019, **7**, 23895–23903.

10 Y. Wang, P. Wang, X. Zhou, C. Li, H. Li, X. Hu, F. Li, X. Liu, M. Li and Y. Song, *Adv. Energy Mater.*, 2018, **8**, 1702960.

11 Q. He, M. Worku, L. Xu, C. Zhou, H. Lin, A. J. Robb, K. Hanson, Y. Xin and B. Ma, *ACS Appl. Mater. Interfaces*, 2020, **12**, 1159–1168.

12 L. Chao, Y. Xia, B. Li, G. Xing, Y. Chen and W. Huang, *Chem.*, 2019, **5**, 995–1006.

13 X. Huang, R. Chen, G. Deng, F. Han, P. Ruan, F. Cheng, J. Yin, B. Wu and N. Zheng, *J. Am. Chem. Soc.*, 2020, **142**, 6149–6157.

14 Z. Wang, L. Zeng, C. Zhang, Y. Lu, S. Qiu, C. Wang, C. Liu, L. Pan, S. Wu, J. Hu, G.

Liang, P. Fan, H. J. Egelhaaf, C. J. Brabec, F. Guo and Y. Mai, *Adv. Funct. Mater.*, 2020, **30**, 2001240.

15 W. Q. Wu, Z. Yang, P. N. Rudd, Y. Shao, X. Dai, H. Wei, J. Zhao, Y. Fang, Q. Wang, Y. Liu, Y. Deng, X. Xiao, Y. Feng and J. Huang, *Sci. Adv.*, 2019, **5**, eaav8925.

16 M. Yang, Z. Li, M. O. Reese, O. G. Reid, D. H. Kim, S. Siol, T. R. Klein, Y. Yan, J. J. Berry, M. F. A. M. van Hest and K. Zhu, *Nat. Energy*, 2017, **2**, 17038.

17 W. Q. Wu, Q. Wang, Y. Fang, Y. Shao, S. Tang, Y. Deng, H. Lu, Y. Liu, T. Li, Z. Yang, A. Gruverman and J. Huang, *Nat. Commun.*, 2018, **9**, 1625.

18 F. Guo, W. He, S. Qiu, C. Wang, X. Liu, K. Forberich, C. J. Brabec and Y. Mai, *Adv. Funct. Mater.*, 2019, **29**, 1900964.

19 J. Ding, Q. Han, Q.-Q. Ge, D.-J. Xue, J.-Y. Ma, B.-Y. Zhao, Y.-X. Chen, J. Liu, D. B. Mitzi and J.-S. Hu, *Joule*, 2019, **3**, 402–416.

20 J. H. Heo, M. H. Lee, M. H. Jang and S. H. Im, *J. Mater. Chem. A*, 2016, **4**, 17636–17642.

21 P. Li, C. Liang, B. Bao, Y. Li, X. Hu, Y. Wang, Y. Zhang, F. Li, G. Shao and Y. Song, *Nano Energy*, 2018, **46**, 203–211.

22 Y. Y. Kim, T. Y. Yang, R. Suhonen, M. Valimaki, T. Maaninen, A. Kemppainen, N. J. Jeon and J. Seo, *Adv. Sci.*, 2019, **6**, 1802094.

23 D.-K. Lee, D.-N. Jeong, T. K. Ahn and N.-G. Park, *ACS Energy Lett.*, 2019, **4**, 2393-2401.

24 Y. Deng, C. H. Van Brackle, X. Dai, J. Zhao, B. Chen and J. Huang, *Sci. Adv.*, 2019, **5**, eaax7537.

25 Q. Liu, Y. Zhao, Y. Ma, X. Sun, W. Ge, Z. Fang, H. Bai, Q. Tian, B. Fan and T. Zhang, *J. Mater. Chem. A*, 2019, **7**, 18275–18284.

26 A. S. Subbiah, F. H. Isikgor, C. T. Howells, M. De Bastiani, J. Liu, E. Aydin, F. Furlan, T. G. Allen, F. Xu, S. Zhumagali, S. Hoogland, E. H. Sargent, I. McCulloch and S. De Wolf, *ACS Energy Lett.*, 2020, **5**, 3034–3040.